Shear viscosity of strongly coupled Yukawa systems

T. Saigo and S. Hamaguchi
Department of Fundamental Energy Science, Kyoto University, Gokasho, Uji, Kyoto 611-0011, Japan

(Received 12 December 2001; accepted 21 January 2002)

With the use of equilibrium molecular dynamics (MD) simulations, shear viscosity of the Yukawa system is evaluated under strongly coupled conditions. In the limit of weak screening, it is confirmed that the obtained Yukawa shear viscosity approaches the previously known shear viscosity of the one-component plasma. It is shown that Yukawa shear viscosities with appropriate normalization follow a simple temperature scaling formula. Yukawa shear viscosities obtained from the present MD simulations are significantly larger than those obtained previously based on a different numerical method. It is argued that the new simulations provide more plausible values for Yukawa shear viscosities than the previously known results. © *2002 American Institute of Physics.* [DOI: 10.1063/1.1459708]

I. INTRODUCTION

A wide variety of systems of charged particles immersed in charge neutralizing media, such as dusty plasmas and colloidal particles in electrolytes, may be modeled by Yukawa systems with good accuracy if they are in thermodynamical equilibrium.[1–9] Yukawa systems consist of particles with charge Q and mass m interacting through the Yukawa (i.e., screened Coulomb) potentials given by

$$\phi(r)=\frac{Q^2}{4\pi\varepsilon_0}\frac{\exp(-k_D r)}{r}. \tag{1}$$

Here r is the separation length of two particles and k_D^{-1} is the screening length due to Debye shielding by the background medium. Especially in the limit of $k_D \to 0$ (i.e., the infinite screening length), the system is known as the one-component plasma (OCP).

Dynamical properties, such as transport coefficients[2–4,10–15] and wave dispersion,[16,17] are some of the most fundamental properties characterizing systems of many particles. To date various authors have studied dynamic properties of the OCP[18–20] and evaluated the self-diffusion coefficient, shear and bulk viscosities and heat conductivities. As to Yukawa systems, some of the transport coefficients have been evaluated only recently. For example, Ohta and one of the authors (S.H.) have recently evaluated self-diffusion coefficients of Yukawa systems using equilibrium MD simulations in a wide range of the parameter space.[13] Sanbonmatsu and Murillo have evaluated shear viscosity coefficients of Yukawa systems using nonequilibrium MD simulations.[14]

Our initial motivation to study Yukawa systems is to understand statistical dynamics for dusty plasmas. In dusty plasmas, particulates are typically charged negatively due to the high mobility of electrons. The screening arises from the formation of a sheath around each particulate by the background plasma.

The goal of the present work is to determine shear viscosity of Yukawa systems using equilibrium MD simulations, i.e., a numerical method different from that used by Sanbonmatsu and Murillo.[14] We initially intended to corroborate the results obtained in Ref. 14 independently, using a different numerical method. It turns out that shear viscosities we have obtained are significantly larger than those given in Ref. 14. Although the cause of this discrepancy is not yet clear, we have some reasons to believe that our simulation results are more plausible than those given in Ref. 14, as will be discussed in this article.

Static properties of Yukawa systems in thermodynamical equilibrium can be characterized by two dimensionless parameters. One is screening parameter $\kappa = k_D a$, i.e., the ratio of interparticle spacing [i.e., Wigner–Seitz radius $a = (3/4\pi n)^{1/3}$ with n being the particle number density] to screening length k_D^{-1} and the other is coupling parameter $\Gamma = Q^2/4\pi\varepsilon_0 a k_B T$, i.e., the ratio of the average Coulomb potential energy $Q^2/4\pi\varepsilon_0 a$ to temperature T (with k_B being the Boltzmann constant). Alternatively, one may use the ratio of the average interparticle potential energy $Q^2 \exp(-\kappa)/4\pi\varepsilon_0 a$ to temperature, i.e., $\Gamma^* = \Gamma \exp(-\kappa)$, to represent the extent of interparticle correlations of the system. In the present work, however, we follow convention and mostly use κ and Γ (rather than Γ^*) as the system parameters. If the average interparticle potential energy is comparable with or greater than the average kinetic energy, the system is referred to as ''strongly coupled,'' which may be characterized by $\Gamma^* > 1$. The critical Γ for the phase transition between fluid and solid states (under constant density conditions) of a Yukawa system is denoted by Γ_m, where the subscript m represents ''melting.'' Table I lists Γ_m for some selected κ, which are taken from Ref. 9.

Dynamical properties such as transport coefficients depend also on characteristic frequencies of the system. We define the Einstein frequency by

$$\omega_E^2 = \frac{1}{3m}\sum_{i\neq j}\Delta\phi(\mathbf{r}_i-\mathbf{r}_j) = \frac{k_D^2}{3m}\sum_{i\neq j}\phi(\mathbf{r}_i-\mathbf{r}_j),$$

where ϕ is the Yukawa potential of Eq. (1), m is the particle mass, the sum is taken over all i except for (fixed) j and all

TABLE I. The critical Γ for the fluid–solid phase transition and the fcc Einstein frequencies.

κ	Γ_m	$\sqrt{3}\omega_E/\omega_p$
0.0	171.8	1.0000
0.1	172.2	0.9972
0.5	181.9	0.9423
1.0	217.4	0.8178
2.0	440.1	0.5315
3.0	1185	0.3047

particles are assumed to be at given crystal structure sites. This represents the harmonic oscillation frequency of a particle around its equilibrium site when all other particles are situated at their equilibrium sites. Note that $\omega_E \to \omega_p/\sqrt{3}$ as $\kappa \to 0$.[21] Here ω_p is the nominal plasma frequency of Yukawa systems, i.e., $\omega_p = \sqrt{Q^2 n/\epsilon_0 m}$. Although ω_E depends on the selected crystal structure, its numerical values for the fcc and bcc crystals differ only less than 1%. Therefore, in the present work, we only use the fcc Einstein frequency for convenience. Table I lists the fcc Einstein frequencies (with respect to $\omega_p/\sqrt{3}$) for selected κ values.

II. NUMERICAL METHODS

In our MD simulations N simulation particles are placed in a cubic box of side L and periodic boundary conditions are imposed on all boundaries in order to emulate the infinitely large system. The pair potential between particle i and particle j (located at $\mathbf{r}_i$ and $\mathbf{r}_j$) in the simulation box is then given by

$$\Phi(\mathbf{r}_{ij}) = \phi(|\mathbf{r}_{ij}|) + \sum_{\mathbf{n}\neq\mathbf{0}} \phi(|\mathbf{r}_{ij} + \mathbf{n}L|) \tag{2}$$

with the Yukawa pair potential $\phi(r)$ of Eq. (1). The infinite sum of ϕ over integer vectors $\mathbf{n}=(l,m,n)$ represents the contribution from all periodic images. Note that the infinite sum converges only if $k_D \neq 0$. In the case $k_D = 0$ it is replaced by the Ewald sum.[22] In our simulations for finite κ, the second term is approximated by a tensor-product spline function.[7]

As units of mass, length, and time, we employ particle mass m, Wigner–Seitz radius a, and plasma frequency $\sqrt{3}\,\omega_p^{-1}$. The equations of motion in dimensionless form are then given by

$$\frac{d^2\boldsymbol{\xi}_k}{d\tau^2} = -\sum_{j\neq k}^{N} \hat{\nabla}\hat{\Phi}(\boldsymbol{\xi}_k - \boldsymbol{\xi}_j) \quad \text{for } k = 1,...,N, \tag{3}$$

where $\tau = \omega_p t/\sqrt{3}$ and $\boldsymbol{\xi}$ are the dimensionless time and positions and $\hat{\nabla}$ is the gradient in $\boldsymbol{\xi}$. The system of equations of motion above are integrated by a predictor-corrector scheme with variable time steps.[6] The MD code used in this article was initially developed by Farouki[6] and later modified by Ohta[13,17] and the present authors.

Straightforward integration of the equations of motion results in simulations under constant-energy (rather than constant-temperature) conditions. In order to attain thermodynamical equilibrium at desired temperature T (i.e., Γ), therefore, we periodically renormalize particle velocities to the prescribed target value for Γ. The statistical average $\langle\rangle$ may be obtained by taking the time average over a sufficiently long time period once the system reaches thermodynamical equilibrium. In the parameter regime we discussed in this work, it is usually sufficient to run the simulation with velocity rescaling for the first 100 time units (i.e., $0 \leqslant \tau \leqslant 100$) in order to force the system to reach thermodynamical equilibrium. To evaluate time-dependent functions (such as the stress autocorrelation function that we discuss below) in thermodynamical equilibrium, we discontinue the velocity rescaling at $\tau = 100$ and then evaluate the desired functions of time under constant–energy calculations for the next 400 time units (i.e., $100 \leqslant \tau \leqslant 500$). Under such conditions, temperature fluctuates and can gradually shift toward a value different from the target value. Therefore the actual system temperature here is defined as its time average. The number of simulation particles used in our simulations presented in this article is $N = 250$ unless otherwise specified.

In thermodynamical equilibrium MD simulations, we use autocorrelation function for the microscopic stress tensor to evaluate shear viscosity. The xy component of the microscopic stress tensor is defined as

$$J^{xy}(t) = \sum_{i=1}^{N} \left[m v_i^x v_i^y + \sum_{j(>i)}^{N} \sum_{\mathbf{n}} \frac{(r_{ij}^{\mathbf{n}})^x (r_{ij}^{\mathbf{n}})^y}{r_{ij}^{\mathbf{n}}} \frac{d}{dr_{ij}^{\mathbf{n}}} \phi(r_{ij}^{\mathbf{n}}) \right], \tag{4}$$

where $\mathbf{r}_{ij}^{\mathbf{n}} \equiv \mathbf{r}_j - \mathbf{r}_i + \mathbf{n}L$ and $r_{ij}^{\mathbf{n}} = |\mathbf{r}_{ij}^{\mathbf{n}}|$. Also $(r_{ij}^{\mathbf{n}})^\alpha$ and v_i^α ($\alpha = x$, y, or z) are the α component of $\mathbf{r}_{ij}^{\mathbf{n}}$ and $\mathbf{v}_i$, and superscripts x, y, and z denote the corresponding components in the ordinary rectangular coordinate system. All quantities are evaluated at time t. Note that $J^{xy} = J^{yx}$. Other components such as J^{yz} are similarly defined.

Let us define the stress autocorrelation function (SAF) as

$$H^{xy}(t) = \langle J^{xy}(t) J^{xy}(0) \rangle.$$

The statistical average $\langle\rangle$ is obtained by taking a time average of function $J^{xy}(s+t)J^{xy}(s)$ over the initial time s. Note that $H^{xy}(t) = H^{yx}(t)$. As mentioned earlier, time averaging of a function is done under microcanonical conditions after the system reaches thermal equilibrium with given target temperature T. Since the actual system temperature under microcanonical conditions is not an exact constant of time, we have to limit the period of averaging in such a way that shift of the system temperature is limited within about 1% of the target temperature. To reduce statistical noise, we run 30 independent MD simulations with randomly chosen initial conditions for each target temperature T and take an average over these 30 runs for each physical quantity.

Since the x, y, and z directions are equivalent (and the system becomes truly isotropic as $N \to \infty$), we have $H^{xy} = H^{yz} = H^{zx}$. Therefore we write $H(t) \equiv H^{xy}(t)$ and use

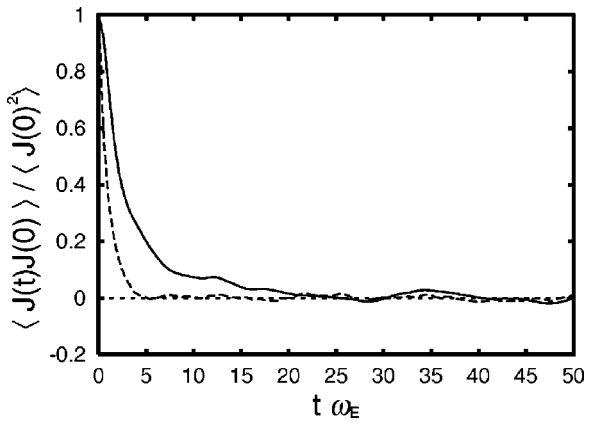

FIG. 1. The SAF $H(t)=\langle J^{xy}(t)J^{xy}(0)\rangle$ versus time for $\kappa=2.0$. The solid line is for $T^*=1.1$ (i.e., $\Gamma=400$) and the dashed line for $T^*=88$ (i.e., $\Gamma=5$).

$H(t)=(H^{xy}+H^{yz}+H^{zx})/3$ to further improve statistics. For example, we show in Fig. 1 the SAF as a function of time (normalized by ω_E^{-1}) for $\kappa=2.0$. The solid line is for $T^*=1.1$ (i.e., $\Gamma=400$) and the dashed line for $T^*=88$ (i.e., $\Gamma=5$). It is seen that the decay time of the SAF is larger for the system with stronger coupling (i.e., larger Γ).

Once the SAF is obtained, the shear viscosity η is given by the Green–Kubo formula, i.e.,

$$\eta=\frac{1}{Vk_BT}\int_0^\infty H(t)dt, \tag{5}$$

where V is the volume of the simulation box.[23] In actual calculations the range of integration above is replaced by $0<\tau<100$, which is sufficiently long in the sense that the contribution of the long-time tail is small compared with statistical noise inherent in our MD simulations with $N=250$.

III. SIMULATION RESULTS

Shear viscosities that we have evaluated from MD simulations using Eq. (5) are given in Tables II and III. The definitions of normalized shear viscosities here are given by

$$\hat{\eta}=\eta/\sqrt{3}mn\omega_E a^2 \quad \text{and} \quad \eta^*=\eta/mn\omega_p a^2,$$

where ω_E and ω_p are the Einstein frequency for fcc crystals and the nominal plasma frequency, as mentioned before. Note that $\hat{\eta}=\eta^*$ when $\kappa=0$. The normalization employed for η^* has been widely used for the OCP as well as some of earlier studies for Yukawa systems. However, as Einstein frequency ω_E, rather than nominal plasma frequency ω_p, is more natural frequency associated with the Yukawa system, we here employ $\hat{\eta}$ as a natural extension of η^* of the OCP in finite screening (i.e., $\kappa\neq0$) cases. Statistical noise for $\hat{\eta}$ is indicated by $\Delta\eta$, which is the standard deviation of values of $\hat{\eta}$ obtained from the 30 simulation runs for a given target temperature T mentioned in the previous section.

As to normalization of temperature, we use the melting temperature T_m, i.e., $T^*\equiv T/T_m=\Gamma_m/\Gamma$, as in Ref. 13. Since shear viscosity is defined only in fluid phase, all the data that we present in this article are for $T^*>1$. Normalized temperature T^* is roughly a measure of how far the system is away from the solid phase.

In Fig. 2 we have plotted $\hat{\eta}$ together with $\Delta\hat{\eta}$ given in Table II for each κ. The solid lines in the figure are fitting curves based on a simple form given by

TABLE II. Shear viscosity of the Yukawa system obtained from MD simulations with $N=250$ simulation particles. The normalized shear viscosities are defined by $\hat{\eta}=\eta/\sqrt{3}mn\omega_E a^2$ and $\eta^*=\eta/mn\omega_p a^2$. Note that $\hat{\eta}=\eta^*$ when $\kappa=0$. Error estimates for $\hat{\eta}$ are indicated by $\Delta\hat{\eta}$ (the definition of which is given in the main text).

κ	Γ	T^*	$\hat{\eta}$	$\Delta\hat{\eta}$	η^*	κ	Γ	T^*	$\hat{\eta}$	$\Delta\hat{\eta}$	η^*
0.1	2.01	85.8	0.503	0.0237	0.502	2.0	1.99	221.0	1.21	0.177	0.646
	5.02	34.3	0.132	0.0134	0.128		4.98	88.4	0.487	0.0583	0.259
	10.0	17.2	0.0687	0.005 17	0.0686		9.92	44.4	0.206	0.0357	0.109
	20.0	8.61	0.0693	0.002 98	0.0691		19.8	22.2	0.110	0.0225	0.0584
	50.0	3.44	0.0912	0.001 50	0.0912		49.0	8.98	0.0976	0.0231	0.0520
	100.0	1.72	0.207	0.0150	0.206		98.9	4.45	0.118	0.0206	0.0628
	150.0	1.15	0.338	0.0318	0.337		199.0	2.21	0.191	0.0220	0.101
							295.0	1.49	0.267	0.0292	0.142
0.5	2.00	91.1	0.531	0.0727	0.500		396.0	1.11	0.352	0.0435	0.187
	5.01	36.3	0.138	0.0169	0.130						
	10.0	18.2	0.0930	0.003 15	0.0874	3.0	5.01	237.0	1.13	0.0100	0.345
	19.9	9.13	0.0670	0.0117	0.0629		9.96	119.0	0.694	0.168	0.211
	50.2	3.63	0.0912	0.009 24	0.0861		19.8	59.9	0.322	0.0220	0.0982
	100.0	1.81	0.204	0.0289	0.192		49.5	24.0	0.202	0.0121	0.0613
	149.0	1.22	0.311	0.0306	0.293		99.3	11.9	0.133	0.008 78	0.0407
							198.0	6.00	0.133	0.0133	0.0406
1.0	2.00	109.0	0.595	0.0330	0.486		395.0	3.00	0.148	0.0191	0.0450
	4.99	43.6	0.210	0.009 70	0.172		996.0	1.19	0.380	0.0337	0.116
	9.90	22.0	0.130	0.0101	0.106						
	19.8	11.0	0.110	0.009 53	0.0904						
	49.4	4.40	0.118	0.0140	0.0964						
	99.0	2.19	0.218	0.0186	0.179						
	199.0	1.09	0.357	0.0258	0.292						

TABLE III. Normalized shear viscosity $\hat{\eta}$ and its kinetic, potential, and cross parts.

κ	T^*	$\hat{\eta}$	$\hat{\eta}_{\rm kin}$	$\hat{\eta}_{\rm pot}$	$\hat{\eta}_{\rm cross}$	κ	T^*	$\hat{\eta}$	$\hat{\eta}_{\rm kin}$	$\hat{\eta}_{\rm pot}$	$\hat{\eta}_{\rm cross}$
0.1	85.8	0.503	0.546	0.0196	−0.0624	2.0	221.0	1.21	1.40	0.0119	−0.192
	34.3	0.132	0.174	0.0353	−0.0803		88.4	0.487	0.532	0.0171	−0.0618
	17.2	0.0687	0.0855	0.0531	−0.0693		44.4	0.206	0.231	0.0312	−0.0565
	8.61	0.0693	0.0424	0.0664	−0.0395		22.2	0.110	0.125	0.0383	−0.0531
	3.44	0.0912	0.0150	0.102	−0.0256		8.98	0.0976	0.0510	0.0733	−0.0263
	1.72	0.207	0.008 37	0.195	0.003 15		4.45	0.118	0.0249	0.108	−0.0150
	1.15	0.338	0.006 87	0.336	−0.004 71		2.21	0.191	0.0123	0.194	−0.0159
							1.49	0.267	0.00907	0.304	−0.0454
0.5	91.1	0.531	0.564	0.0246	−0.0583		1.11	0.352	0.00716	0.394	−0.0495
	36.3	0.138	0.176	0.0310	−0.0687						
	18.2	0.0930	0.114	0.0502	−0.0716	3.0	237.0	1.13	1.29	0.0171	−0.174
	9.13	0.0670	0.0391	0.0630	−0.0353		119.0	0.694	0.647	0.0248	0.0204
	3.63	0.0912	0.0202	0.0976	−0.0262		59.9	0.322	0.320	0.0314	−0.0288
	1.81	0.204	0.009 53	0.203	−0.008 20		24.0	0.202	0.140	0.0606	0.001 10
	1.22	0.311	0.006 41	0.308	−0.003 96		11.9	0.133	0.0544	0.0745	0.004 73
							6.00	0.133	0.0330	0.111	−0.0106
1.0	109.0	0.595	0.797	0.0192	−0.225		3.00	0.148	0.0169	0.146	−0.0151
	43.6	0.210	0.232	0.0285	−0.0502		1.19	0.380	0.007 74	0.367	0.005 66
	22.0	0.130	0.113	0.0388	−0.0219						
	11.0	0.110	0.0524	0.0624	−0.003 98						
	4.40	0.118	0.0206	0.0993	−0.002 15						
	2.19	0.218	0.0109	0.161	0.0467						
	1.09	0.357	0.006 93	0.359	−0.008 95						

$$\hat{\eta} = aT^* + \frac{b}{T^*} + c. \tag{6}$$

The values of a, b and c are summarized in Table IV. It is shown that the normalized viscosity has a minimum at $T^* \simeq 10$ for all κ examined here.

It is interesting to note that these fitting parameters depend on κ very weakly, suggesting that normalized η is almost independent of κ. In Fig. 3 all the data given in Table II are plotted in a single chart. The solid line is the fitting curve of form Eq. (6) for all these data points. [The fitting parameters are given in the last row (indicated as κ being "all") of Table IV.] The fitting is excellent, especially for $1 \leqslant T^* \lesssim 3$ and $T^* \gtrsim 50$. For intermediate T^* ($\simeq 10$), however, $\hat{\eta}$ for larger κ is observed to be slightly but systematically higher than that for smaller κ. Therefore, although the "universal" curve shown in Fig. 3 represents the dependence of $\hat{\eta}$ on T^* very well for all κ examined here, care must be taken if the curve is used to evaluate shear viscosity values near the viscosity minimum.

Universality of the curve given in Fig. 3 indicates the κ dependence of shear viscosity $\eta = \sqrt{3} mn\omega_E a^2 \hat{\eta}$ for given temperature T comes from the κ dependence of ω_E and T_m. Self-diffusion coefficients of Yukawa systems[13] have similar nature, i.e., the normalized self-diffusion coefficient $\mathcal{D} = D/\omega_E a^2$ with D being the dimensional self-diffusion coefficient is known to follow a "universal" curve as a function of T^* when T^* is relatively small in fluid phase (i.e., $1 < T^* \lesssim 10$).

We now look into details of shear viscosity. Let us separate the stress tensor $\mathbf{J}(t)$ into two parts as $\mathbf{J}(t) = \mathbf{J}_{\rm kin}(t) + \mathbf{J}_{\rm pot}(t)$, where the $\alpha\beta$ component of kinetic part $\mathbf{J}_{\rm kin}$ is defined as $J^{\alpha\beta}_{\rm kin}(t) = \Sigma_{i=1}^{N} m v_i^{\alpha} v_i^{\beta}$, i.e., the first term of Eq. (4). This represents momentum transport by the displacement of particles. Similarly, the potential part $\mathbf{J}_{\rm pot}$, which is defined as the second term of Eq. (4), represents momentum transport by collisions.

Using the definitions above, we also define the kinetic, potential, cross parts of shear viscosity as

$$\eta_{\rm kin} = \frac{1}{Vk_BT} \int_0^{\infty} \langle J^{xy}_{\rm kin}(t) J^{xy}_{\rm kin}(0) \rangle,$$

$$\eta_{\rm pot} = \frac{1}{Vk_BT} \int_0^{\infty} \langle J^{xy}_{\rm pot}(t) J^{xy}_{\rm pot}(0) \rangle,$$

$$\eta_{\rm cross} = \frac{2}{Vk_BT} \int_0^{\infty} \langle J^{xy}_{\rm kin}(t) J^{xy}_{\rm pot}(0) \rangle,$$

respectively. The shear viscosity is then given by the sum of these terms, i.e., $\eta = \eta_{\rm kin} + \eta_{\rm pot} + \eta_{\rm cross}$. The kinetic and potential parts of shear viscosity, once normalized by $\sqrt{3} mn\omega_E a^2$, follow scaling laws independent of κ, as shown momentarily.

Figure 4 shows the normalized kinetic part of shear viscosity, i.e., $\hat{\eta}_{\rm kin} \equiv \eta_{\rm kin}/\sqrt{3} mn\omega_E a^2$, as a function of normalized temperature T^*. The solid line is the fitting curve given by $\hat{\eta}_{\rm kin} = 0.00592 T^*$. It is shown that numerically obtained $\hat{\eta}_{\rm kin}$ essentially follows this function, almost independent of κ, in the parameter regime discussed here.

Figure 5 shows the normalized potential part of shear viscosity, i.e., $\hat{\eta}_{\rm pot} \equiv \eta_{\rm pot}/\sqrt{3} mn\omega_E a^2$, as a function of normalized temperature T^*. The solid line is a fitting curve given by $0.402/T^*$ and the dashed line is a fitting curve given by $0.212/\sqrt{T^*}$. The cross point of these two functions is around $T^* \simeq 3$.

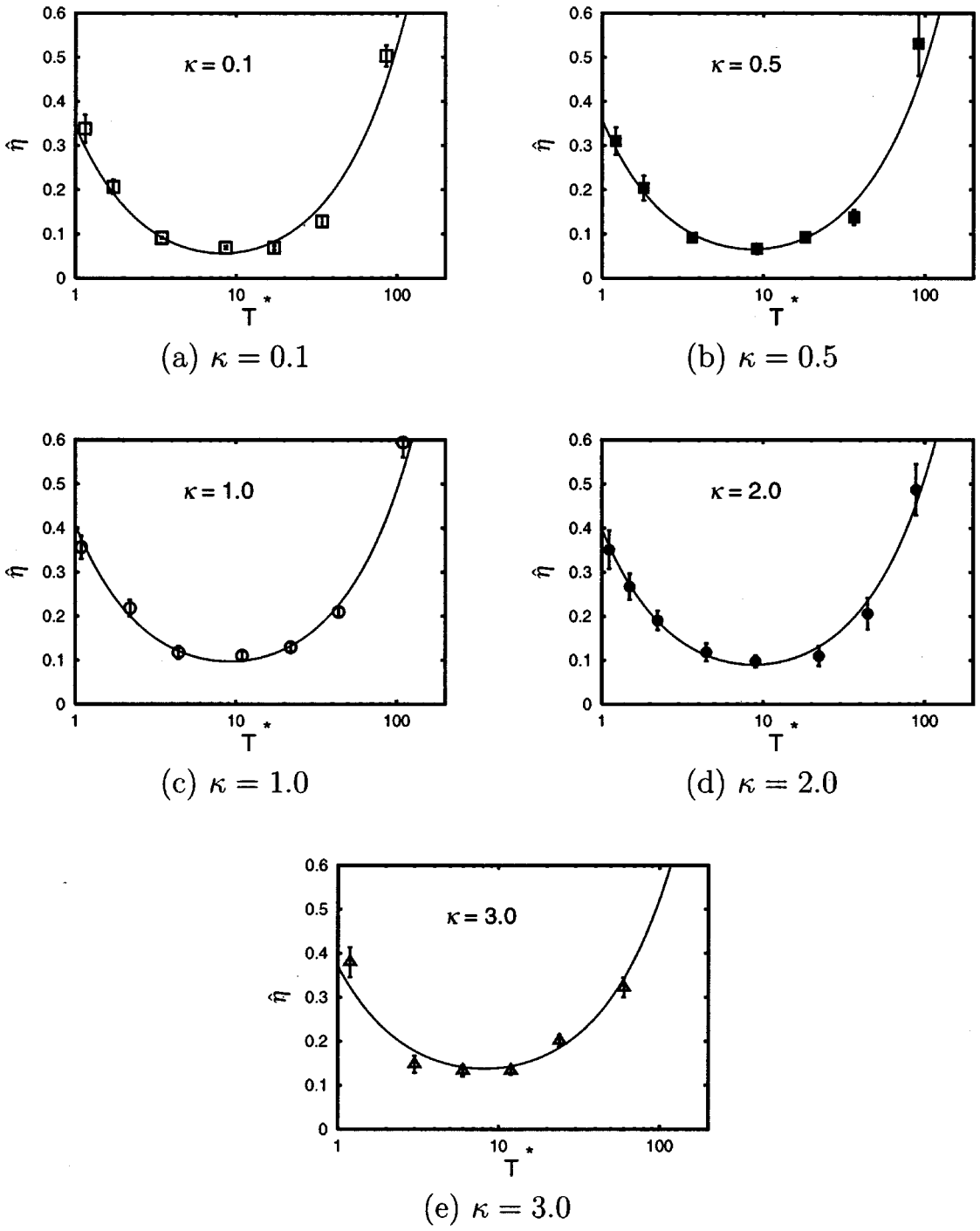

FIG. 2. Normalized shear viscosity $\hat{\eta}$ for various κ. The solid lines are fitting curves given by Eq. (6). The vertical bars represent standard deviation $\Delta\hat{\eta}$.

Unlike $\hat{\eta}_{\mathrm{kin}}$ or $\hat{\eta}_{\mathrm{pot}}$, the normalized cross part $\hat{\eta}_{\mathrm{cross}} \equiv \eta_{\mathrm{cross}}/\sqrt{3}mn\omega_E a^2$, seems to depend on κ as well as T^*. As shown in Table III, the cross part is relatively small compared with the other two parts, especially if $T^*<3$ or $T^*>50$. This results in good agreement of numerically obtained $\hat{\eta}$ values with the scaling curve given in Fig. 3, especially for $T^*<3$ and $T^*>50$. However, for intermediate T^*, $\hat{\eta}_{\mathrm{cross}}$ becomes comparable with other parts, which results in slight deviation of the curve from the data points near the viscosity minimum, as we have pointed out before.

TABLE IV. The fitting parameters a, b, and c for the normalized viscosity given by Eq. (6), obtained from our simulation data shown in Table II.

κ	a	b	c
0.1	0.005 56	0.373	−0.0347
0.5	0.005 04	0.375	−0.0212
1.0	0.004 71	0.393	0.0113
2.0	0.005 09	0.393	0.000 596
3.0	0.004 56	0.303	0.0634
all	0.004 96	0.324	−0.0133

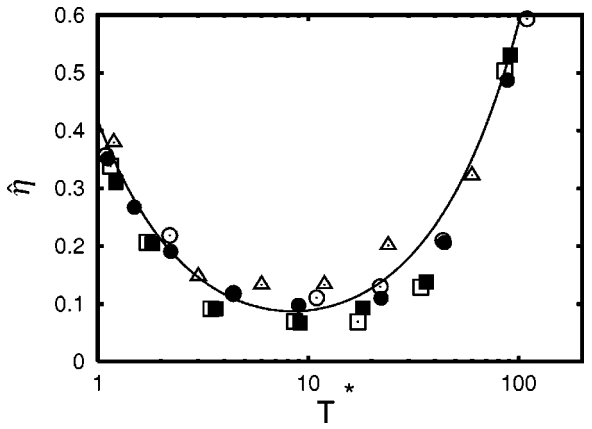

FIG. 3. Normalized shear viscosity $\hat{\eta}$ versus normalized temperature T^*. The solid line is the fitting curve based on Eq. (6) with fitting parameters given in Table IV (under "all"). Here □: $\kappa=0.1$, ■: $\kappa=0.5$, ○: $\kappa=1.0$, ●: $\kappa=2.0$, and △: $\kappa=3.0$.

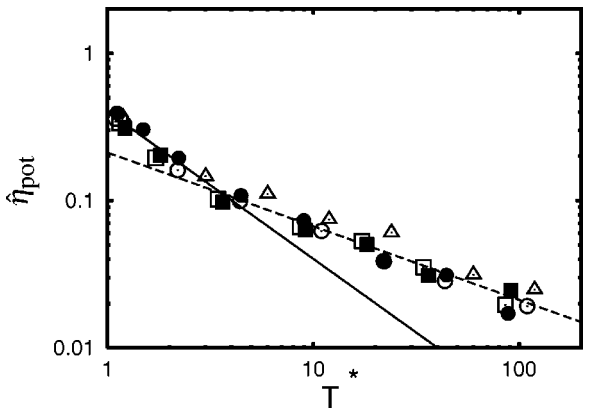

FIG. 5. The potential part of shear viscosity $\hat{\eta}_{pot}$ as a function of normalized temperature T^*. The solid line is the fitting curve given by $0.402/T^*$ and the dashed line is the fitting curve given by $0.212/\sqrt{T^*}$. Here □: $\kappa=0.1$, ■: $\kappa=0.5$, ○: $\kappa=1.0$, ●: $\kappa=2.0$, and △: $\kappa=3.0$, as in Fig. 3.

IV. DISCUSSION

To demonstrate that our simulation results smoothly approach data for the OCP as $\kappa\to 0$, we have plotted in Fig. 6 shear viscosity values of the OCP previously obtained by various authors[18–20] and our simulations results for $\kappa=0.1$ together with the fitting curve given in Fig. 3. Note that, in this figure, we have plotted η^*, instead of $\hat{\eta}$. It is seen that our simulation results for $\kappa=0.1$ are sufficiently close to those for the OCP, as expected.

In order to confirm that the number of particles $N=250$ that we employed in our MD simulations is sufficient to provide reasonably accurate estimates of shear viscosity values, we have performed simulations with different N values (up to $N=1000$). Figure 7 shows numerically obtained shear viscosity as a function of $1/N$ for $\kappa=2.0$ and target $\Gamma=400$. (Note that, for each case, numerically obtained actual Γ, which is the time average of fluctuating Γ, is slightly different from the target value 400. As mentioned before, the difference is typically within 1%.) The solid line is the least-square fit, which suggests that $\hat{\eta}=0.407$ at $N=\infty$. It is seen that errors incurred by employing (relatively small) $N=250$ are roughly within 20%, which is comparable with typical statistical noise in our simulations.

Recently, Sanbonmatsu and Murillo have evaluated shear viscosity of Yukawa systems for $1\leqslant\kappa\leqslant 4$ using nonequilibrium molecular dynamics (NEMD) simulations.[14] The shear viscosity values they have obtained (expressed in terms of η^* in Ref. 14) are typically $\frac{1}{2}$–$\frac{1}{3}$ of those we have presented in this work. The difference is significant, much larger than possible errors due to statistical noise or relatively small N that we used in our simulations. While Sanbonmatsu and Murillo did not check whether their MD simulations provide shear viscosity values that smoothly approaches those for the OCP if $\kappa\to 0$, Rosenfeld[15] has shown that shear viscosity values of the OCP obtained by Donko and Nyiri and those for all $\kappa>1$ obtained by Sanbonmatsu and Murillo follow two different curves when they are plotted as $\eta^*\Gamma_m^{1/2}$ vs Γ/Γ_m $(=1/T^*)$. We also note that, compared with the scaling of $\hat{\eta}$ vs T^* that we have presented in this article (which the results by Donko and Nyiri also follow), the results by

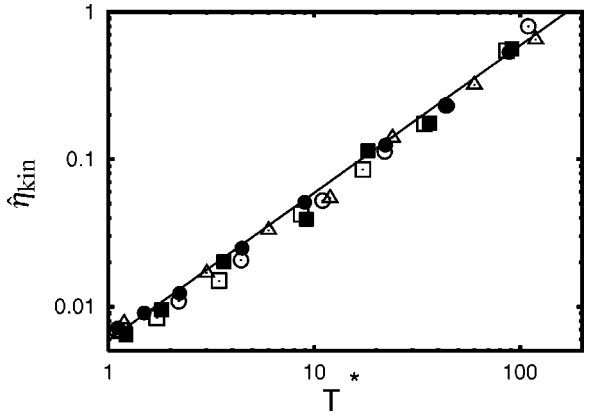

FIG. 4. The kinetic part of shear viscosity $\hat{\eta}_{kin}$ as a function of normalized temperature T^*. The solid line is the fitting curve given by $\hat{\eta}_{kin}=0.005\,92T^*$. Here □: $\kappa=0.1$, ■: $\kappa=0.5$, ○: $\kappa=1.0$, ●: $\kappa=2.0$, and △: $\kappa=3.0$, as in Fig. 3.

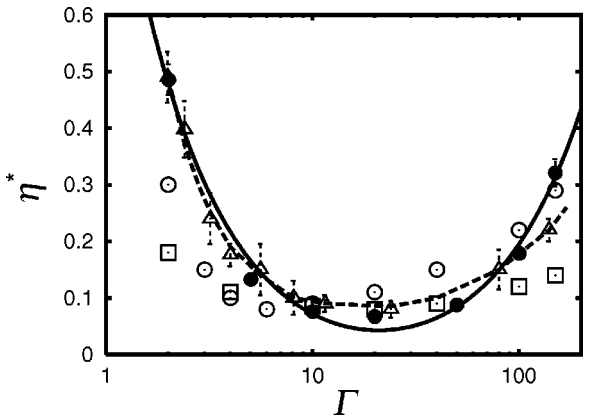

FIG. 6. Comparison of numerically obtained shear viscosities: our simulation results for $\kappa=0.1$ (denoted by ●) and simulation results for the OCP (i.e., $\kappa=0$) obtained by Vieillefosse and Hansen (□), Wallenborn and Baus (○) and Donko and Nyiri (△). The solid line is the fitting curve based on Eq. (6) with fitting parameters given in Table IV (under "all"). The broken line is the fitting function for △.

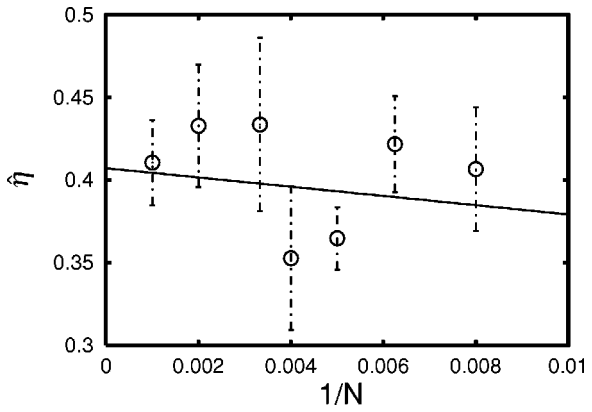

FIG. 7. Dependence of the shear viscosity on $1/N$, i.e., the inverse of the number of simulation particles, for $\kappa=2.0$ and $\Gamma=400$.

Sanbonmatsu and Murillo provide a different (i.e., lower) scaling curve. Furthermore we have confirmed that our results as well as the results by Donko and Nyiri also follow the same scaling suggested by Rosenfeld.[15] Although the cause of the discrepancy between our results (based on equilibrium MD simulations) and those given in Ref. 14 (based on NEMD simulations) is not clear at the moment, if we believe there is a simple universal scaling law for shear viscosity, as in the case of self-diffusion coefficients,[13,15] our estimates of shear viscosity for Yukawa systems seem more plausible.

In summary, we have estimated shear viscosity of the strongly coupled Yukawa system for various screening lengths $(0.1\leqslant\kappa\leqslant 3)$, using the Green–Kubo formula and thermodynamical equilibrium MD simulations. Especially, in the limit of weak screening $(\kappa\rightarrow 0)$, we have confirmed that the obtained Yukawa shear viscosity approaches that of the one–component plasma (OCP) previously obtained by other authors. As in the case of self-diffusion coefficients, if we employ the inverse of Einstein frequency ω_E (rather than the nominal plasma frequency ω_p) as the time unit and normalize the shear viscosity accordingly, we have shown that the normalized shear viscosity $\hat{\eta}$ as a function of the normalized temperature $T^*=T/T_m$ follows a simple universal scaling function that is independent on κ.

Note added in proof. It has come to our attention that independent work on the evaluation of Yukawa shear viscosity by Salin and Caillol has been published recently.[24] We have confirmed their results are in good agreement with our results presented here.

ACKNOWLEDGMENTS

The authors gratefully acknowledge helpful discussions with H. Ohta and M. S. Murillo.

This work is supported by the Grant In Aid For Scientific Research by the Ministry of Education, Culture, Sports, Science and Technology.

[1] S. Hamaguchi, Plasmas Ions **2**, 57 (1999).
[2] R. O. Rosenberg and D. Thirumalai, Phys. Rev. A **33**, 4473 (1986).
[3] K. Kremer, M. O. Robbins, and G. S. Grest, Phys. Rev. Lett. **57**, 2694 (1986).
[4] M. O. Robbins, K. Kremer, and G. S. Grest, J. Chem. Phys. **88**, 3286 (1988).
[5] S. Hamaguchi and R. T. Farouki, J. Chem. Phys. **101**, 9876 (1994).
[6] R. T. Farouki and S. Hamaguchi, J. Chem. Phys. **101**, 9885 (1994).
[7] R. T. Farouki and S. Hamaguchi, J. Comput. Phys. **115**, 276 (1994).
[8] S. Hamaguchi, R. T. Farouki, and D. H. E. Dubin, J. Chem. Phys. **105**, 7641 (1996).
[9] S. Hamaguchi, R. T. Farouki, and D. H. E. Dubin, Phys. Rev. E **56**, 4671 (1997).
[10] G. Zerah, J. Clerouin, and E. L. Pollock, Phys. Rev. Lett. **69**, 446 (1992).
[11] J. Clerouin, E. L. Pollock, and G. Zerah, Phys. Rev. A **46**, 5130 (1992).
[12] Y. Rosenfeld, E. Nardi, and Z. Zinamon, Phys. Rev. Lett. **75**, 2490 (1995).
[13] H. Ohta and S. Hamaguchi, Phys. Plasmas **7**, 4506 (2000).
[14] K. Y. Sanbonmatsu and M. S. Murillo, Phys. Rev. Lett. **86**, 1215 (2001).
[15] Y. Rosenfeld, J. Phys.: Condens. Matter **13**, 39 (2001).
[16] G. Kalman, M. Rosenberg, and H. E. De Witt, Phys. Rev. Lett. **84**, 6030 (2000).
[17] H. Ohta and S. Hamaguchi, Phys. Rev. Lett. **84**, 6026 (2000).
[18] P. Vieillefosse and J. P. Hansen, Phys. Rev. A **12**, 1106 (1975).
[19] J. Wallenborn and M. Baus, Phys. Rev. A **18**, 1737 (1978).
[20] Z. Donko and B. Nyiri, Phys. Plasmas **7**, 45 (2000).
[21] K. I. Golden, G. Kalman, and P. Wyns, Phys. Rev. A **46**, 3454 (1992).
[22] P. P. Ewald, Ann. Phys. **64**, 253 (1921).
[23] J. M. Haile, *Molecular Dynamics Simulation* (Wiley, New York, 1992).
[24] G. Salin and J.-M. Caillol, Phys. Rev. Lett. **88**, 065002 (2002).